Publ. Astron. Soc. Japan (2016) 68 (5), 90 (1–20)
doi: 10.1093/pasj/psw081

Large X-ray flares on stars detected with MAXI/GSC: A universal correlation between the duration of a flare and its X-ray luminosity

Yohko Tsuboi,[1,*] Kyohei Yamazaki,[1] Yasuharu Sugawara,[1] Atsushi Kawagoe,[1] Soichiro Kaneto,[1] Ryo Iizuka,[1,2] Takanori Matsumura,[1] Satoshi Nakahira,[3] Masaya Higa,[1] Masaru Matsuoka,[3,4] Mutsumi Sugizaki,[3] Yoshihiro Ueda,[5] Nobuyuki Kawai,[3,6] Mikio Morii,[6] Motoko Serino,[3] Tatehiro Mihara,[3] Hiroshi Tomida,[4] Shiro Ueno,[4] Hitoshi Negoro,[7] Arata Daikyuji,[8] Ken Ebisawa,[2] Satoshi Eguchi,[9] Kazuo Hiroi,[5] Masaki Ishikawa,[10] Naoki Isobe,[11] Kazuyoshi Kawasaki,[4] Masashi Kimura,[12] Hiroki Kitayama,[12] Mitsuhiro Kohama,[4] Taro Kotani,[13] Yujin E. Nakagawa,[3] Motoki Nakajima,[14] Hiroshi Ozawa,[7] Megumi Shidatsu,[5] Tetsuya Sootome,[3,15] Kousuke Sugimori,[6] Fumitoshi Suwa,[7] Hiroshi Tsunemi,[12] Ryuichi Usui,[6] Takayuki Yamamoto,[3,7] Kazutaka Yamaoka,[13] and Atsumasa Yoshida[3,13]

[1]Department of Physics, Faculty of Science and Engineering, Chuo University, 1-13-27 Kasuga, Bunkyo-ku, Tokyo 112-8551, Japan
[2]Institute of Space and Astronautical Science (ISAS), Japan Aerospace Exploration Agency (JAXA), 3-1-1 Yoshino-dai, Chuo-ku, Sagamihara, Kanagawa 252-5210, Japan
[3]MAXI team, RIKEN, 2-1 Hirosawa, Wako, Saitama 351-0198, Japan
[4]ISS Science Project Office, Institute of Space and Astronautical Science (ISAS), Japan Aerospace Exploration Agency (JAXA), 2-1-1 Sengen, Tsukuba, Ibaraki 305-8505, Japan
[5]Department of Astronomy, Kyoto University, Kitashirakawa-Oiwake-cho, Sakyo-ku, Kyoto, Kyoto 606-8502, Japan
[6]Department of Physics, Tokyo Institute of Technology, 2-12-1 Ookayama, Meguro-ku, Tokyo 152-8551, Japan
[7]Department of Physics, Nihon University, 1-8-14 Kanda-Surugadai, Chiyoda-ku, Tokyo 101-8308, Japan
[8]Department of Applied Physics, University of Miyazaki, 1-1 Gakuen Kibanadai-nishi, Miyazaki, Miyazaki 889-2192, Japan
[9]National Astronomical Observatory of Japan, 2-21-1, Osawa, Mitaka, Tokyo 181-8588, Japan
[10]School of Physical Science, Space and Astronautical Science, The Fraduate University for Advanced Studies (Sokendai), 3-1-1 Yoshino-dai, Chuo-ku, Sagamihara, Kanagawa 252-5210, Japan
[11]Institute of Space and Astronautical Science (ISAS), Japan Aerospace Exploration Agency (JAXA), 3-1-1 Yoshino-dai, Chuo-ku, Sagamihara, Kanagawa 252-5210, Japan
[12]Department of Earth and Space Science, Osaka University, 1-1 Machikaneyama, Toyonaka, Osaka 560-0043, Japan
[13]Department of Physics and Mathematics, Aoyama Gakuin University, 5-10-1 Fuchinobe, Chuo-ku, Sagamihara, Kanagawa 252-5258, Japan
[14]School of Dentistry at Matsudo, Nihon University, 2-870-1 Sakaecho-nishi, Matsudo, Chiba 101-8308, Japan

[15]Department of Electronic Information Systems, Shibaura Institute of Technology, 307 Fukasaku, Minuma-ku, Saitama, Saitama 337-8570, Japan

*E-mail: tsuboi@phys.chuo-u.ac.jp

Received 2016 February 12; Accepted 2016 July 29

Abstract

Twenty-three giant flares from thirteen active stars (eight RS CVn systems, one Algol system, three dMe stars, and one young stellar object) were detected during the first two years of our all-sky X-ray monitoring with the gas propotional counters (GSC) of the Monitor of All-sky X-ray Image (MAXI). The observed parameters of all these MAXI/GSC flares are found to be at the upper ends for stellar flares with the luminosity of 10^{31-34} erg s^{-1} in the 2–20 keV band, the emission measure of 10^{54-57} cm^{-3}, the *e*-folding time of 1 hr to 1.5 d, and the total radiative energy released during the flare of 10^{34-39} erg. Notably, the peak X-ray luminosity of $5^{+4}_{-2} \times 10^{33}$ erg s^{-1} in the 2–20 keV band was detected in one of the flares on II Peg, which is one of the, or potentially the, largest-ever-observed in stellar flares. X-ray flares were detected from GT Mus, V841 Cen, SZ Psc, and TWA-7 for the first time in this survey. Whereas most of our detected sources are multiple-star systems, two of them are single stars (YZ CMi and TWA-7). Among the stellar sources within 100 pc distance, the MAXI/GSC sources have larger rotation velocities than the other sources. This suggests that the rapid rotation velocity may play a key role in generating large flares. Combining the X-ray flare data of nearby stars and the sun, taken from literature and our own data, we discovered a universal correlation of $\tau \propto L_X^{0.2}$ for the flare duration τ and the intrinsic X-ray luminosity L_X in the 0.1–100 keV band, which holds for 5 and 12 orders of magnitude in τ and L_X, respectively. The MAXI/GSC sample is located at the highest ends of the correlation.

Key words: stars: activity — stars: flare — stars: late-type — stars: rotation — stars: variables: general

1 Introduction

Cool stars, which have spectral types of F, G, K, and M, are known to show X-ray flares. The flares are characterized by a fast-rise and slow-decay light curve. The flares generally accompany the rise and decay in the plasma temperature. The general understanding, based on the numerous studies of solar flares, is that such features arise as the consequence of a sudden energy release and relaxation process in the reconnection of magnetic fields on/around stellar surfaces. In solar flares, the reconnection, which occurs at large coronal heights, accelerates primarily electrons (and possibly ions) up to MeV energies, and the electrons precipitate along the magnetic fields into the chromosphere, suddenly heating the plasma at the bottom of the magnetic loop to very high temperatures. A large amount of plasma streams from the bottom to the top of the magnetic loop, while cooling has already started by that time. The flare temperature thus peaks before the emission measure (*EM*) does, or analogously, harder emission peaks before softer emission.

Numerous studies on flare stars have been made with pointing observations. For the reviews, see Pettersen (1989), Haisch, Strong, and Rodono (1991), Favata and Micela (2003), Güdel (2004), and references therein. However, we cannot yet answer some fundamental questions, such as how large a flare a star can have, and how very large flares are generated. The poor understanding is rooted in the fact that the larger flares occur less frequently. Hence, all-sky monitoring is crucial to detect such large flares.

X-ray all-sky monitors such as Ariel-V/SSI, GRANAT/WATCH, and Swift/BAT have detected some large stellar flares. Using the data of Ariel-V/SSI spanning 5.5 years, Pye and McHardy (1983) and Rao and Vahia (1987) detected a total of 20 flares from 17 stellar sources, including 10 RS CVn systems and seven dMe stars. Rao and Vahia (1987) showed that there is a positive correlation between the bolometric luminosity and the X-ray peak luminosity. GRANAT/WATCH detected two X-ray transients, which have a counterpart of a flare star in their respective positional error boxes

(Castro-Tirado et al. 1999). Swift with BAT prompted the follow-up observations with XRT after detecting large flares from an RS CVn system II Peg (Osten et al. 2007) and that from a dMe star EV Lac (Osten et al. 2010). Flares from two other RS CVn stars (CF Tuc and UX Ari) have been detected with Swift/BAT (Krimm et al. 2013).

Following successful detections of large flares with all-sky X-ray surveys, we executed a survey of stellar flares with the Monitor of All-sky X-ray Image (MAXI: Matsuoka et al. 2009). MAXI is a mission of an all-sky X-ray monitor operated in the Japanese Experiment Module (JEM; Kibo) on the International Space Station (ISS) since 2009 August. It observes an area in the sky once per 92-minute orbital cycle, and enables us to search for stellar flares effectively. In this paper, we report the results with the gas proportional counters (GSC) of MAXI obtained by the first two years of operation from 2009 August to 2011 August. The results found with the CCD camera of MAXI (SSC) will be given elsewhere. We describe the MAXI observation in section 2, our flare-search method and the results in section 3, then discuss the properties of the detected flares and the flare sources in section 4.

2 Observations

The MAXI has two types of slit cameras, the GSC and SSC, which incorporate X-ray detectors consisting of gas proportional counters and of X-ray CCDs, respectively. These detectors cover energy ranges of 2 to 30 keV and of 0.5 to 12 keV, respectively (Matsuoka et al. 2009; Tsunemi et al. 2010; Tomida et al. 2011; Mihara et al. 2011). As stated in section 1, the observations of stellar flares examined here were conducted by the GSC, which has a larger field of view (FoV) and then sky coverage than SSC. The GSC achieves better sensitivity in the 2–10 keV band than any other X-ray all-sky monitors using large-area proportional counters with a low background so far, and therefore is preferable for detecting stellar flares. The data from 2009 August 15 to 2011 August 15 are used here.

The GSC consists of 12 pieces of proportional counters, which employ resistive carbon-wire anodes to acquire one-dimensional position sensitivity. Each set of two counters forms a single camera unit, of which the GSC has six in total. The overall FoV is a slit shape of $160^\circ \times 3^\circ$ in the horizon and zenith directions, respectively, which allows the MAXI to scan the entire sky twice as the ISS moves; i.e., MAXI/GSC can scan 97% of the entire sky with each ISS orbit. When the ISS passes high background regions such as the South Atlantic Anomaly, the high voltage of the GSC is switched off to protect the proportional counters from damage. Then, the actual sky coverage is about 85% of the whole sky per 92-minute orbital period, 95% per day, and 100% per week.

The point spread function (PSF) in the anode-wire direction is determined by the angular response of the slit-and-slat collimator and the positional response of the position-sensitive gas counter along the anode wire. The collimator is designed to have an angular resolution of $1\overset{\circ}{.}0$–$1\overset{\circ}{.}5$ in full width at half maximum (FWHM), depending on the X-ray incident angle in the anode-wire direction and on the X-ray energy. The PSF in the scan direction is determined with the modulated time variations of the detector area, which changes according to the triangular transmission function of the collimator during each transit. The GSC typically scans a point source on the sky during a transit of 40–150 s with a FoV of $1\overset{\circ}{.}5$ width (FWHM) every 92-minute orbital period. The transit time depends on the source incident angle in the anode-wire direction. The detector area for the target changes according to the triangular transmission function of the collimator during each transit. The peak value is 4–5 cm^2 per camera. The detailed performance of the GSC was described by Sugizaki et al. (2011). All the data we used were delivered from the MAXI database system (Negoro et al. 2016).

3 Analysis and results

3.1 Search for flaring stars

In order to search for flares from stars, we used the alert system "nova search" (Negoro et al. 2010). The alert system on the ground swiftly reports X-ray transient events to astronomers worldwide, prompting potential follow-up observations. For a further search, we have created movies of the GSC image for each sky area segmented into circles of 10° radii, setting the observation time of one day for one shot. The entire sky is covered by about 200 segments.

From the confirmed transient events, we selected the events whose peaks are located within 2° from nearby known stellar sources. The source lists are composed of the catalogs of Torres et al. (2006), López-Santiago et al. (2006), and Riedel et al. (2014). The locations of the X-ray peaks are determined automatically for the sources confirmed by "nova search", or by eye from the movies for the others. For these selected stellar-flare candidates, we proceeded to the following identification process.

3.2 Significance in source detection

We estimated the significance of a detected source with the same method as employed in Uzawa et al. (2011), as follows: (1) events within a circle with $1\overset{\circ}{.}5$ radius centered at the transient event ("source region") in the 2–10 keV band are extracted; (2) ∼10 circle regions, whose radii are all 1°.5, are chosen around the source region ("background circles"); (3) the number of events in the 2–10 keV band in each background circle is counted; (4) the average of the counts in a background circle is defined as the background level; (5) the standard deviation of the counts in a background circle is regarded as the $1\,\sigma$ background fluctuation; (6) the background level is subtracted from the count in the source region, and the residual is regarded as the source count; (7) the source counts divided by the $1\,\sigma$ background fluctuation is defined as the source significance.

In the first flare on II Peg (FN15 in table 1) on 2009 August 20, the source was in a high-noise area, located close to the wire edge. Thus, we set the background circles in the high-noise area in order to estimate the appropriate level of the background. The time-spans, for which we extracted the data, are indicated in the light curves with horizontal bars in figure 1.

3.3 Reconfirmation of the source positions

The number of the stellar flare candidates with significance larger than $5\,\sigma$ level were 23 in total. For these flares, we further performed two-dimensional image fittings to obtain the precise error regions for the X-ray positions. The fitting algorithm is given in Morii et al. (2010). The shape of the region can be approximated with an ellipse with the typical semi-major and semi-minor axes of 0°.7 and 0°.5, respectively, at 90% confidence level. We found that all the error regions still encompass the position of each stellar counterpart in our list, which we had seen within 2° from the X-ray peak. We also confirmed that all the stellar counterparts are listed in the ROSAT bright source catalog (Voges et al. 1999). No other ROSAT bright-sources are in the same error regions for all the events but one; the error region of FN20 (see table 1) encompasses AT Mic (1RXS J204151.2−322604) and 1RXS J204257.5−320320. 1RXS J204257.5−320320 is not in our list of nearby sources, and the detailed nature is not known. Moreover, certainly no X-ray variation has ever been reported. Then we regard that the transient occurred on the established flare star, AT Mic. The dates of each flare, the error regions, the X-ray count rates, the significant levels, and the stellar counterparts are summarized in table 1.

The 23 detected flares were found to come from 13 stars: eight RS CVn systems (VY Ari, UX Ari, HR 1099, GT Mus, V841 Cen, AR Lac, SZ Psc, and II Peg), one Algol-type star (Algol), three dMe stars (AT Mic, EQ Peg, and YZ CMi), and one YSO (TWA-7). Note that the detection of the flare from TWA-7 has already been reported in Uzawa et al. (2011). We list the fundamental parameters of the stellar counterparts in table 2. Four out of 13 sources showed flares multiple times. We adopt the source distances listed in table 2 when we estimate or discuss the physical parameters in this paper. These distances are all within 100 pc, except that of GT Mus (172 pc). Figure 2 displays the relation between the source distance and the X-ray luminosity L_{X}. This implies that our detection limit is roughly 10 mCrab in the 2–20 keV band.

3.4 Timing analysis

Figure 1 shows the GSC light-curves of all the detected flares in the 2–10 keV band. In making the light-curves, the data for the sources were extracted from the circles with the radius ranging from 1°.3 to 1°.7, which is selected depending on the signal-to-noise ratio. The backgrounds are extracted from the annuli with the inner and outer radii of 2° and 4°, respectively, except for the following two cases, in which an edge of a wire is close to the source region. In the case of the flare on HR 1099 (FN5) on 2010 January 23, we chose the background region as an annulus with the inner and outer radii of 2° and 3°.5, respectively, to eliminate a high-noise area. As for the first flare on II Peg (FN15) on 2009 August 20, since the source was more closely located near a wire edge than in the HR 1099 case, the source region was just in the high-noise area. Thus, in order to remove the appropriate level of the background, we chose the background region as a rectangle of 3°.4 × 19°, removing a central circle with 1°.7 radius. After subtracting the background, we normalized all the extracted source-counts by dividing the data in the source region by the total exposure (in units of cm^2 s), which is obtained with a time integral of the collimator effective area. We fitted them with a burst model, which is described as a linear rise followed by an exponential decay. The *e*-folding times are shown in table 3 and figure 3, which range from about 1 hr (AR Lac) to 1.5 d (GT Mus).

3.5 Spectral analysis

We also analyzed X-ray spectra in flare phases. The GSC spectra were extracted during the time interval indicated with the horizontal bars on the light curves (figure 1), as those used in the estimation of the significance of source detection. We used the same source and background regions as in the timing analysis. Since the photon-statistics are limited, we fitted the spectra with a simple model: a thin-thermal plasma model (*mekal*: Mewe et al. 1985, 1986; Kaastra 1992; Liedahl et al. 1995) with the fixed abundance ratios of heavy elements to the solar values. We ignored the interstellar absorption, since all the sources are located within 200 pc and are not in famous molecular clouds. An

Table 1. Date and other observed parameters of each flare.

Flare	MJD *	UT *	Error Ellipse				Count rate†	Significance	Counterpart	Category
		(YYYY MMM DD HH:MM:SS)	Center (J2000.0) (HH:MM:SS, DDD:MM:SS)	Semimajor axis (°)	Semiminor axis (°)	Roll angle (°)	(10^{-2} counts s^{-1})	(σ)		
FN1	55144.347	2009 Nov 09 08:19:15	02:49:55.49, +31:18:32.34	1.0	0.82	90	1.1	7.4	VY Ari	RS CVn
FN2	55080.193	2009 Sep 06 04:37:45	03:26:33.38, +28:31:36.03	0.6	0.57	90	0.72	9.5	UX Ari	RS CVn
FN3	55662.965	2011 Apr 11 23:09:50	03:26:06.13, +28:49:51.75	0.31	0.26	0	12	14	UX Ari	RS CVn
FN4	55678.049	2011 Apr 27 01:10:25	03:26:09.44, +28:47:41.58	0.44	0.36	110	32	16	UX Ari	RS CVn
FN5	55219.221	2010 Jan 23 05:18:10	03:37:02.86, +00:42:24.30	0.5	0.43	170	17	24	HR1099	RS CVn
FN6	55244.054	2010 Feb 17 01:17:51	03:36:28.02, +00:23:58.80	0.43	0.39	90	0.53	7.1	HR1099	RS CVn
FN7	55503.647	2010 Nov 03 15:31:35	03:39:24.90, +00:19:37.43	1.1	0.73	40	4.5	5.1	HR1099	RS CVn
FN8	55625.878	2011 Mar 05 21:03:45	03:36:24.15, +00:31:51.98	0.31	0.21	12	47	29	HR1099	RS CVn
FN9	55510.015	2010 Nov 11 00:21:07	11:40:43.67, −65:01:44.00	0.44	0.35	15	0.27	10	GT Mus	RS CVn
FN10	55769.137	2011 Jul 27 03:16:43	14:34:07.69, −60:33:54.43	0.49	0.32	0	58	8.7	V841 Cen	RS CVn
FN11	55219.255	2010 Jan 23 06:06:55	22:08:29.83, +45:38:19.77	0.64	0.54	75	22	17	AR Lac	RS CVn
FN12	55376.647	2010 Jun 29 15:31:51	22:06:42.49, +45:40:20.19	0.75	0.56	130	19	6.7	AR Lac	RS CVn
FN13	55785.823	2011 Aug 12 19:45:20	22:14:56.90, +46:15:13.01	2.4	0.96	45	0.71	5.2	AR Lac	RS CVn
FN14	55101.059	2009 Sep 28 01:25:30	23:11:50.76, +02:55:10.28	0.53	0.49	15	3.5	5.7	SZ Psc	RS CVn
FN15	55063.937	2009 Aug 20 22:29:55	23:58:33.24, +28:15:57.20	1.1	0.97	45	2.0	19	II Peg	RS CVn
FN16	55291.166	2010 Apr 05 03:58:30	23:54:58.71, +28:51:27.99	0.74	0.64	20	41	13	II Peg	RS CVn
FN17	55433.679	2010 Aug 25 16:17:55	23:55:01.76, +28:36:48.00	1.1	0.7	153	1.2	9.9	II Peg	RS CVn
FN18	55434.315	2010 Aug 26 07:34:00	23:57:52.31, +28:39:34.00	1.2	9.5	0	0.29	9.6	II Peg	RS CVn
FN19	55561.057	2010 Dec 31 01:22:00	03:07:57.26, +40:50:15.00	0.46	0.33	10	20	11	Algol	Algol
FN20	55613.840	2011 Feb 21 20:10:00	20:43:34.04, −32:13:03.96	0.56	0.52	45	69	19	AT Mic	dMe
FN21	55574.278	2011 Jan 13 06:41:00	23:31:33.68, +19:43:53.94	0.35	0.32	40	36	15	EQ Peg	dMe
FN22	55628.897	2011 Mar 08 21:31:00	07:43:46.70, +03:26:26.16	0.32	0.29	160	39	45	YZ CMi	dMe
FN23	55446.767	2010 Sep 07 18:25:00	10:43:41.64, −33:36:30.75	0.57	0.45	150	14	17	TWA 7	YSO

*Modified Julian Date and Universal Time when the maximum luminosity was observed.
†Observed count rate in the 2–10 keV band.

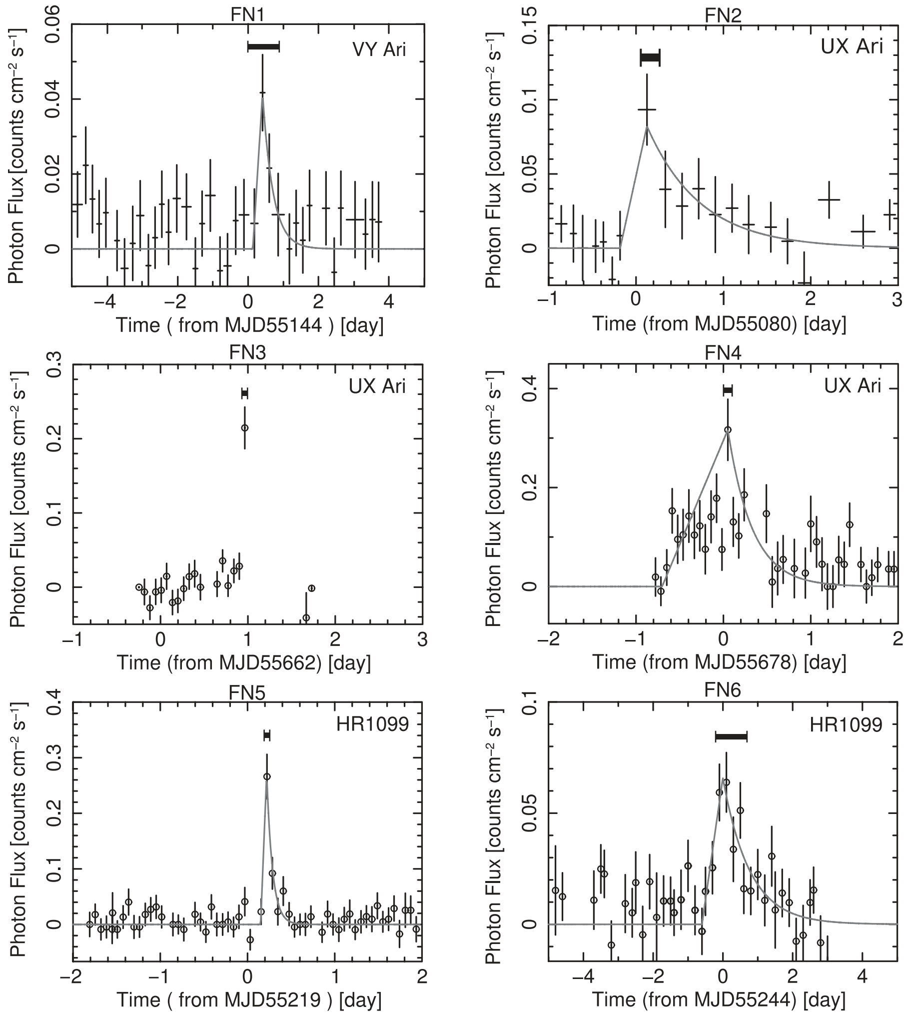

Fig. 1. Light curves of 23 flares. The data are extracted in the 2–10 keV band. Each data set shown by open circles is made from one orbit data, while the data sets in the panels for FN1, 2, 9, and 14 are binned with the data of multiple orbits. The horizontal bar(s) above the major line peak(s) in each panel is the time interval, from which the data are extracted to derive the detection significances and to make the spectral analysis. The light curve of TWA-7 is from Uzawa et al. (2011).

example of a spectrum with the best-fitting model is found in the figure 2 in Uzawa et al. (2011). Table 3 and figure 3 give the best-fitting parameters and the distribution of the derived properties (EM, L_X, e-folding time, the total energy), respectively.[1]

4 Discussion

4.1 Detected flares and the source categories

We detected 23 flares, whose X-ray luminosities are 10^{31-34} erg s^{-1} in the 2–20 keV band and the emission measures are 10^{54-57} cm^{-3}. The flares released the energy of 10^{34-39} erg radiatively with the e-folding times of 1 hr to 1.5 d (see figure 3). All the detected flares are from active stars; that is, eight RS CVn systems, one Algol system, three dMe stars, and one YSO, totaling 13 stars. This confirms that RS CVn systems and dMe stars are intense flare sources, as reported in Pye and McHardy (1983) and Rao and Vahia (1987). The X-ray flares from GT Mus, V841 Cen, SZ Psc, and TWA-7 were detected for the first time in this survey. Notably, II Peg showed the L_X of $5^{+4}_{-2} \times 10^{33}$ erg s^{-1} in the 2–20 keV band at the peak of the flare, which is one of the largest-ever-observed stellar flares.

Most of the flare sources that we detected with MAXI/GSC are multiple-star systems (see table 2). However, two of them were single stars: TWA-7 (Uzawa et al. 2011) and YZ CMi. In addition, two other (AT Mic and EQ Peg), though they are binary systems, have a very wide

[1] One might guess that significantly different results may be obtained with different plasma models, such as *apec* (Smith et al. 2001). Therefore, we fitted the spectra of FN5, FN9 and FN16 with the *apec* model and found that the obtained parameters (kT, EM, L_X) were consistent with each other between the *mekal* and *apec* models for a wide range of temperature.

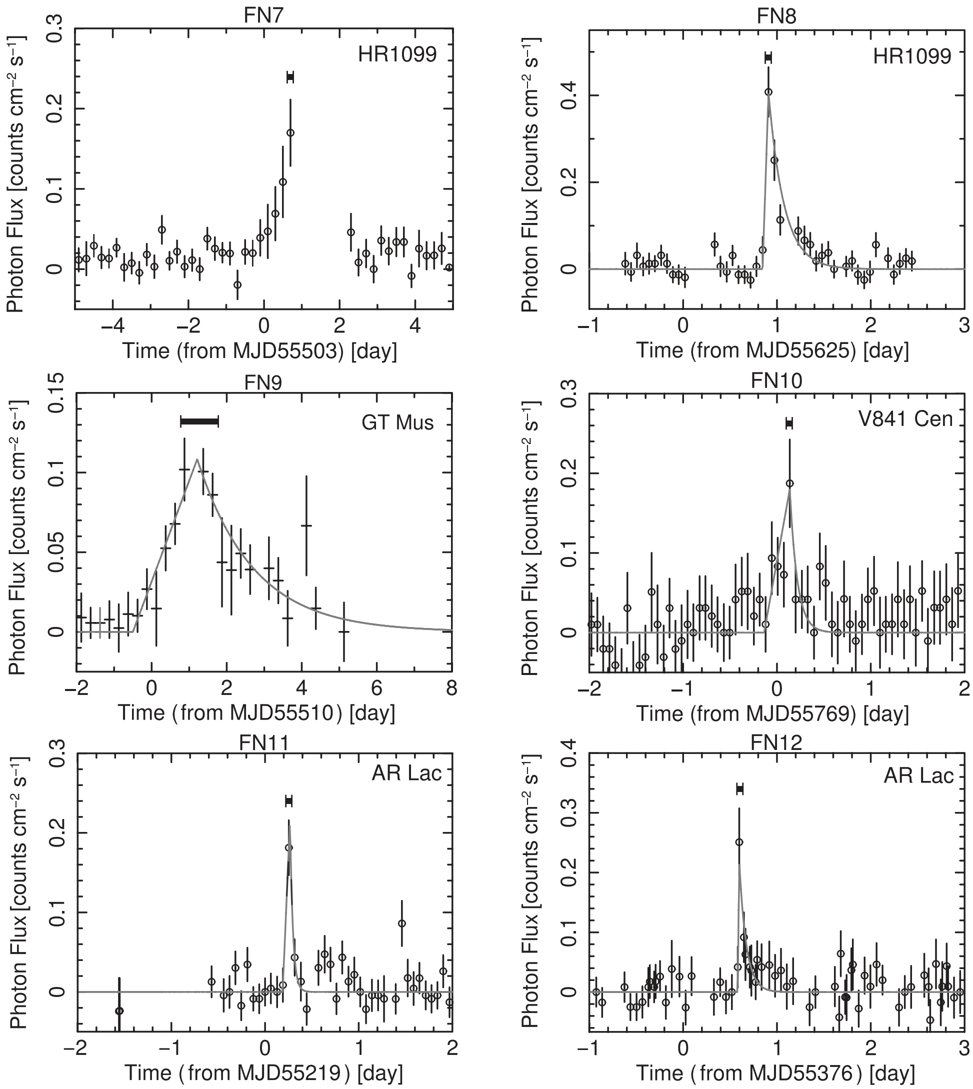

Fig. 1. (Continued)

binary-separation of roughly 6000 $R_\odot$, and so are practically the same as single stars. All of these four stars are known to have no accretion disk. These results reinforce the scenario that neither binarity (e.g., Getman et al. 2011), nor accretion (e.g., Kastner et al. 2002; Argiroffi et al. 2011), nor star–disk interaction (e.g., Hayashi et al. 1996; Shu et al. 1997; Montmerle et al. 2000) is essential to generating large flares, as already discussed in Uzawa et al. (2011).

According to the catalog of active binary stars (Eker et al. 2008), 256 active binaries (e.g., RS CVn binaries, dMe binaries, etc.) are known within the distance of 100 pc from the solar system. However, we have detected flares from only 10 out of them. Four of them (UX Ari, HR 1099, AR Lac, and II Peg) have exhibited flares more than twice.

4.2 X-ray activity on solar-type stars

As for the solar-type stars, 15 G-type main-sequence stars are known within the 10 pc distance (from the "AFGK 'bright' stars within 10 pc" webpage[2]). The MAXI/GSC has not detected any X-ray flares from these stars. The nearest G-type star is α Cen A (G2 V) at a distance of 1.3 pc (Söderhjelm 1999). An upper limit to the L_X of α Cen A is estimated to be 2×10^{28} erg s^{-1}, based on the detection limit of 10 mCrab with MAXI/GSC. This is consistent with the X-ray luminosity observed in solar flares: L_X is mostly lower than 10^{27}–10^{28} erg s^{-1} (Feldman et al. 1995). However, large X-ray flares with respective L_X's of 10^{29} erg s^{-1} and of 2×10^{31} erg s^{-1} have been observed from

[2] ⟨http://www.solstation.com/stars/pc10afgk.htm⟩.

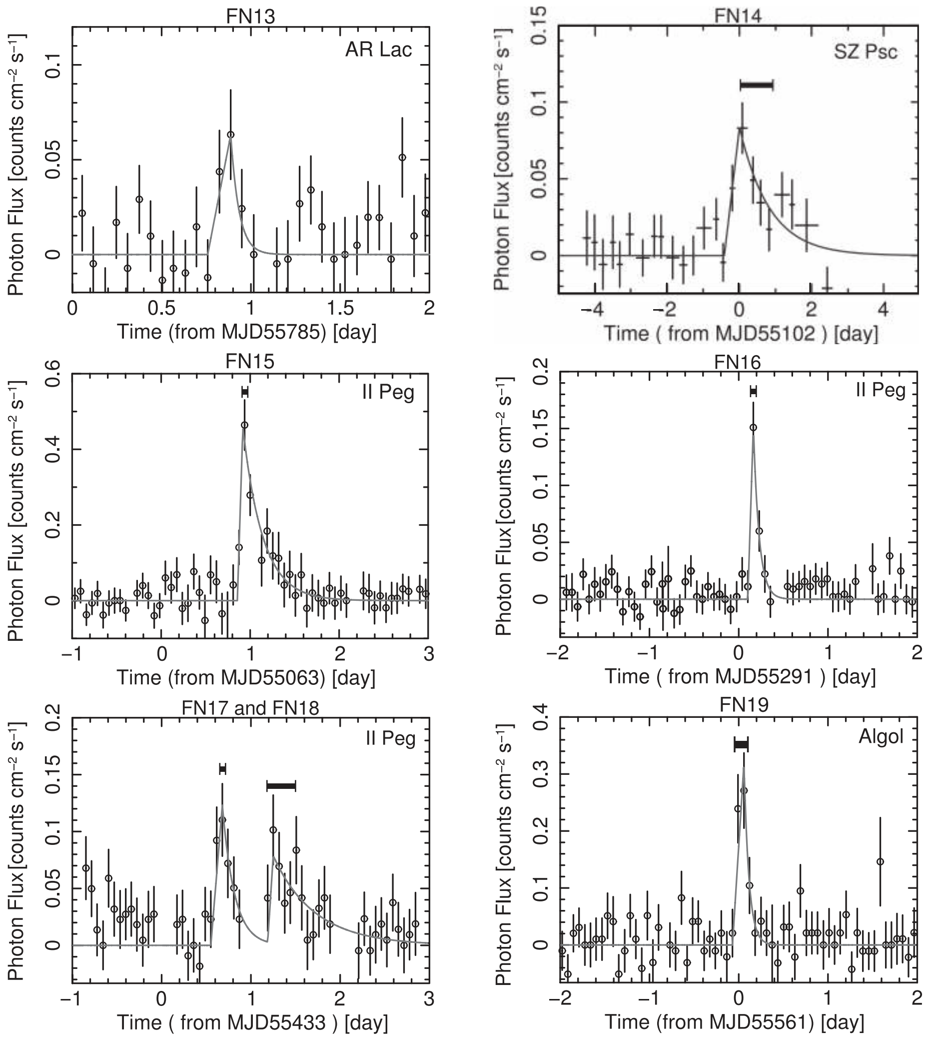

Fig. 1. (Continued)

ordinary solar-type stars π^1 UMa (Landini et al. 1986) and BD +10°2783 (Schaefer et al. 2000). Schaefer, King, and Deliyannis (2000) called such flares "superflares." So far, very few extensive studies have been made in the X-ray band and provided any good constraints on the frequency of the occurrence of "superflares" in the band. Our MAXI/GSC two-year survey is the best X-ray study of this kind. From our result, we can claim that the flares with L_{X} of larger than 1×10^{30} erg s^{-1} must be very rare for solar-type stars.

4.3 *EM* vs. *kT* and the derived loop parameters

Figure 4 shows a plot of *EM* vs. plasma temperature (kT) for the flares in our study of the MAXI/GSC sources, together with solar flares (Feldman et al. 1995), solar microflares (Shimizu 1995), and flares from the stars in literature (see table 4 for the complete set of references). All of the plotted samples are roughly on the universal correlation over orders of magnitude (Feldman et al. 1995; Shibata & Yokoyama 1999). Our sample is located at the high end of the correlation for both the temperatures and the emission measures.

Now, we consider the two important physical parameters of flares; that is, the size and the magnetic field. Shibata and Yokoyama (1999) formulated the theoretical *EM*–*kT* relations for a given set of a loop-length and magnetic field as equations (5) and (6) in their paper (see figure 4 for a few representative cases).[3] We calculated the loop-length and magnetic-field strength for each of the observed flares with MAXI-GSC, based on these relations

[3] Shibata and Yokoyama (1999)'s calculation of the *EM*–*kT* relations is based on the magnetohydrodynamic numerical simulations of the reconnection by Yokoyama and Shibata (1998). The simulation takes account of heat conduction and chromospheric evaporation on the following four assumptions: (1) the plasma volume is equal to the cube of the loop length; (2) the gas pressure of the confined plasma in the loop is equal to the magnetic pressure of the reconnected loop; (3) the observed temperature at the flare peak is one-third of the maximum temperature at the flare onset; (4) the pre-flare proton (= electron) number density outside the flare loop is 10^9 cm^{-3}.

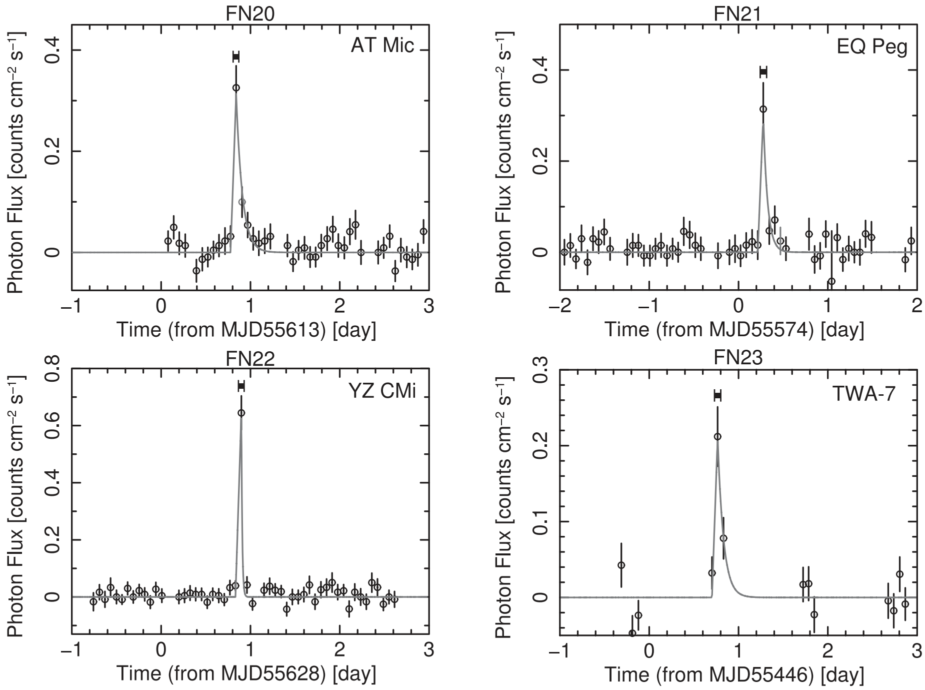

Fig. 1. (Continued)

(Shibata & Yokoyama 1999), as listed in table 3. The magnetic field of our sample is comparable with those of flares on the Sun (∼15–150 G). On the other hand, our sample has flare loops that are of orders of magnitude larger than those on the Sun ($<0.1\,R_\odot$). Especially noteworthy loop length among our sample are the two largest flares relative to their binary separations, FN4 from UX Ari and FN16 from II Peg. Their loop lengths are 10 and 20 times larger than their respective binary separations, which are unprecedentedly large among stellar flares.

The extraordinary large loop lengths could possibly be an artifact of the systematic error in the model by Shibata and Yokoyama (1999). In fact, their derived loop lengths are 10 times larger than those obtained by Favata, Micela, and Reale (2001), who used a hydrodynamic model from Reale and Micela (1998). In Shibata and Yokoyama (2002), which is the follow-up paper of Shibata and Yokoyama (1999), it is argued that their derived loop length could be reduced to roughly 1/10 if the two assumptions [(3) and (4) mentioned in footnote 3] are altered. In our MAXI sample, even if the true loop sizes are 1/10 of the above-estimated values as a conservative case, the largest sizes are 0.2–5 times larger than their binary separations and so are still large.

4.4 Duration vs. X-ray luminosity

We search for potential correlations in various plots to study what deciding factors are for the generation of large stellar flares and to what extent. Figure 5 plots the duration of flares ($\tau_{\rm lc}$) vs. the intrinsic X-ray luminosity ($L_{\rm X\_bol}$) in the 0.1–100 keV band for the stars detected with MAXI/GSC and with other missions (see table 4 for the complete set of references). Here, we have introduced $L_{\rm X\_bol}$ in order to take all the radiative energy into our calculation.[4] Solar flares (Pallavicini et al. 1977; Shimizu 1995; Veronig et al. 2002) are also superposed.[5] The data points of the MAXI/GSC flares are found to be located at the highest ends in both the $L_{\rm X\_bol}$ and the duration axes among all the stellar flares. The plot indicates that there is a universal correlation between $L_{\rm X\_bol}$ of a flare and its duration, such that a longer duration means a higher $L_{\rm X\_bol}$. Remarkably, the correlation holds for wide ranges of parameter values for $10^{22} \lesssim L_{\rm X\_bol} \lesssim 10^{34}$ erg s^{-1} and $10^1 \lesssim \tau_{\rm lc} \lesssim 10^6$ s. Using the data sets of the stellar flares detected with MAXI (this work) and other missions (see table 4) and the solar flares reported by Pallavicini, Serio, and Vaiana (1977), we fitted

[4] See the Appendix for the detailed process to derive $L_{\rm X\_bol}$ for each data set.

[5] As the duration, we used the *e*-folding time for each flare in our work and the works introduced in table 4. For the data of Pallavicini, Serio, and Vaiana (1977) and that of Veronig et al. (2002), we used "decay time," the definitions of which are up to the corresponding authors. For the data of Shimizu (1995), we used the duration itself in FWHM reported in that paper. Generally, flares in any magnitude have fast-rise and slow-decay light curves, and the longest rise times are comparable to the corresponding decay times (e.g., Pallavicini et al. 1977; Imanishi et al. 2003). Therefore the samples are consistent with one another within a factor of 2, or 0.3 in the same logarithmic scale as in the vertical axis of figure 5.

Table 2. General properties of stars in our sample.

Object name	HD	Spectral type	Rotation velocity (km s^{-1})	Radius ($R_\odot$)	a sin$i$* ($R_\odot$)	Inclination of orbit (°)	e	Distance (pc)	References†
VY Ari	17433	K3 V + K4 IV§	10.2	1.90	8.2	57	0.085	44	(1)(2)(3)(4)
UX Ari	21242	G5 V + K0 IV§	41.5	5.78	5.9 (h)/5.3 (c)	59.2	0	50.2	(3)(4)(5)(6)
HR1099	22468	G5 IV + K1 IV§	59.0	3.30	1.9 (h)/2.4 (c)	38	0	29	(4)(7)(8)(9)(10)
GT Mus	101379	(A0V+A2V) + (G5III+G8III§)	—	33.0	15	10	0.032	172	(4)(11)(12)(13)
V841 Cen‡	127535	K1 IV§	—	3.8	4.1	—	0	63	(14)(15)(16)
AR Lac	210334	G2 IV + K0 IV§	73.7	2.68	4.6 (h)/4.5 (c)	89.4	0	42	(3)(4)(17)(18)(19)
SZ Psc	219113	F5 IV + K1 IV§	80.2	6.0	8.7 (h)/6.4 (c)	69.8	0	88	(3)(4)(20)(21)
II Peg	224085	K2 IV§ + M0–3 V	—	2.21	4.9	60	0	42	(4)(22)(23)(24)(25)
Algol	19356	B8 V + K2 IV§	—	3.4	14	81.4	0	28.5	(26)(27)(28)(29)
AT Mic	196982	M4.5 V + M4.5 V§	24.6	0.38	5980	—	—	10.2	(30)(31)(32)(33)
EQ Peg	—	M3.5 V + M5 V§	88.5	0.35	5590	30	—	6.5	(34)(35)(36)(37)(38)
YZ CMi	—	M4.5 V§	5.3	0.29	—	—	—	5.9	(31)(34)(39)
TWA-7	—	M2 V§	19.2	1.89	—	—	—	27	(40)(41)

*The a and i in a sin$i$ show the semi-major axis and the inclination angle, respectively. The (h) and (c) show the semi-major axes for the orbit of the hot and cool components, respectively.

†(1) Alekseev and Kozlova (2001), (2) Bopp et al. (1989), (3) Glebocki and Stawikowski (1995), (4) ESA (1997), (5) Carlos and Popper (1971), (6) Duemmler and Aarum (2001), (7) Donati et al. (1997), (8) Donati (1999), (9) Fekel (1983), (10) Lanza et al. (2006), (11) Murdoch et al. (1995), (12) Randich, Gratton, and Pallavicini (1993), (13) Stawikowski and Glebocki (1994), (14) Özeren, Doyle, and Jevremovic (1999), (15) Strassmeier, Paunzen, and North (1994), (16) Collier (1982), (17) Chambliss (1976), (18) Zboril et al. (2005), (19) Sanford (1951), (20) Eaton and Henry (2007), (21) Jakate et al. (1976), (22) Berdyugina et al. (1998), (23) Marino et al. (1999), (24) O'Neal et al. (2001), (25) Vogt (1981), (26) Richards et al. (2003), (27) Sarna (1993), (28) Singh, Drake, and White (1995), (29) van den Oord and Mewe (1989), (30) Lim, Vaughan, and Nelson (1987), (31) Mitra-Kraev (2007), (32) Mitra-Kraev et al. (2005), (33) Wilson (1978), (34) Morin et al. (2008), (35) Pallavicini, Tagliaferri, and Stella (1990a), (36) Pettersen, Coleman, and Evans (1984), (37) Pizzolato et al. (2003), (38) Hopmann (1958), (39) Reiners, Basri, and Browning (2009), (40) Mamajek (2005), (41) Yang, Johns-Krull, and Valenti (2008).

‡V841 Cen is a single-lined RS CVn binary.

§The stellar component with the symbol § has the largest radius in the multiple-star system. As for the values for the radius and the rotation velocity in this table, the components with this symbol are used.

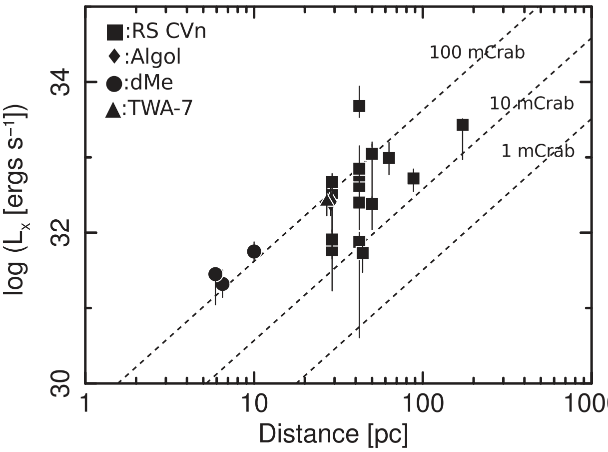

Fig. 2. Log–log plot of X-ray luminosity in the 2–20 keV band of flares vs. distance from active stars detected with MAXI/GSC. The filled squares, filled diamond, filled circles, and filled triangle show RS-CVn type stars, Algol, dMe stars, and TWA-7, respectively. The detection limit appeared to be roughly 10 mCrab in the 2–20 keV band.

the data with a linear function in the log–log plot and obtained the best-fitting function of

$$\tau_{\rm lc} = (1.1^{+4.7}_{-0.9}) \times 10^4 \left(\frac{L_{\rm X\_bol}}{10^{33}\ {\rm erg\ s^{-1}}}\right)^{0.20\pm0.03} \ {\rm s}, \quad (1)$$

where the errors of both the coefficient and the power are in 1σ confidence level.[6] The best-fitting model is shown with a solid line in figure 5, top panel. We found that the best-fitting model agrees also with the range of the data for solar microflares reported by Shimizu (1995), even though the luminosities $L_{\rm X\_bol}$ of their data are smaller than $\sim 10^{25}$ erg s^{-1}, whereas those used for our fitting are larger than that.

For comparison, Veronig et al. (2002) and Christe et al. (2008) have derived similar power-law slopes to ours, $\sim$0.33 for the GOES data and $\sim$0.2 for the RESSI data, respectively, though with the limited energy bands. The ranges of their luminosities are $L_{\rm X} = 10^{23.5\text{–}25.5}$ erg s^{-1} in the 3.1–24.8 keV band and $L_{\rm X} = 10^{22.5\text{–}25.5}$ erg s^{-1} in the 6–12 keV band.

In the following subsections, we discuss the plausible models to explain this positive correlation, examining three potentially viable scenarios: the radiative-cooling dominant, the conductive-cooling dominant, and the propagating-flare models. Note that we have chosen the former two models for simplicity and examine them separately, although it is expected, as most star-flare models assume, that both radiation and conduction are present in a flare and that the latter is active early in the decay and the former is, later (e.g., Shibata & Yokoyama 2002; Cargill & Klimchuk 2004; Reale 2007). We assume that the duration of a flare, $\tau_{\rm lc}$, represents the cooling time of the heated plasma when we examine the radiative- and conductive-cooling dominant models.

4.4.1 Radiative-cooling model

First, we consider the condition where the radiative cooling is dominant. Since the thermal energy is lost via radiation, $\tau_{\rm lc}$ and the radiative cooling time $\tau_{\rm rad}$ are given by

$$\tau_{\rm lc} \simeq \tau_{\rm rad} = \frac{3n_{\rm e}kT}{n_{\rm e}^2 F(T)} = \frac{3kT}{n_{\rm e} F(T)}, \quad (2)$$

where $n_{\rm e}$ and $F(T)$ are the electron density and the radiative loss rate, respectively. We obtained the radiative loss rate, using the *CHIANTI* atomic database (version 8.0) and the *ChiantiPy* package (version 0.6.4).[7]

On the other hand, based on the plot of EM vs. kT (figure 4), we confirm that most of the observed data of stellar and solar flares are confined in the region of 15 G $< B <$ 150 G, where B is magnetic field strength. The region is mathematically described as

$$EM \simeq 10^{48} \alpha^{-5} \left(\frac{T}{10^7\ {\rm K}}\right)^{17/2} {\rm cm^{-3}}, \quad (3)$$

where α is a non-dimensional parameter ranging between 0.3 and 3. Since the derived EM and $F(T)$ compose $L_{\rm X\_bol}$ as

$$L_{\rm X\_bol} = EM\, F(T), \quad (4)$$

we obtain, combining it with equation (3),

$$L_{\rm X\_bol} \simeq 10^{48} \alpha^{-5} \left(\frac{T}{10^7\ {\rm K}}\right)^{17/2} F(T). \quad (5)$$

Once both $\tau_{\rm lc}$ and $L_{\rm X\_bol}$ were parametrized with the temperature T, we inserted solid lines in figure 5 as their relation for the radiative-cooling dominant model.

Observationally, the electron density $n_{\rm e}$ was measured to be 10^{11} cm^{-3} in flares of Proxima Centauri with a high-resolution spectroscopy in the X-ray band (Güdel et al. 2002). In the solar flares, $n_{\rm e}$ of $10^{10\text{–}11}$ cm^{-3} has been calculated from the EM and the volume of the loop (Pallavicini et al. 1977). Some other spectroscopic observations of solar flares have indicated a wide range of $n_{\rm e}$; $10^{11\text{–}13}$ cm^{-3} (see references in Güdel 2004). Therefore, we derived the permitted ranges for radiative-cooling plasma in the following two cases: (1) $n_{\rm e} = 10^{11}$ cm^{-3} and $\alpha = 0.3$–3 (figure 5, middle panel), (2) $n_{\rm e} = 10^{10\text{–}13}$ cm^{-3} and $\alpha = 1$ (figure 5, bottom panel). With the wide permitted range, the figures

[6] Shimizu (1995) and Veronig et al. (2002) presented the plots which indicate the X-ray luminosity and duration of each flare, but without tables that give the exact values. Thus we excluded both data sets from the fitting.

[7] ⟨http://www.chiantidatabase.org/chianti.html⟩.

Table 3. Best-fitting parameters in the fitting, and derived flare parameters.*

	kT	EM	Flux†	$L_{X(2-20)}$‡	χ^2_ν (d.o.f)	τ_d§	E_{tot}‖	l♯		B**
	(keV)	(10^{54} cm^{-3})	(10^{-10} erg cm^{-2} s^{-1})	(10^{31} erg s^{-1})		(ks)	(10^{35} erg)	($R_\odot$)	(Binary separation)	(G)
FN1	5	1	2	5	0.42 (4)	26	10	4	0.4	50
	(2–40)	(0.5–2)	(1–3)	(3–7)		(11–50)	(8–20)	(0.1–20)	(0.01–2)	(10–3000)
FN2	4	24	8	20	1.7 (7)	53	100	30	2	20
	(2–30)	(15–36)	(4–10)	(10–30)		(30–81)	(60–200)	(1–100)	(0.1–8)	(8–600)
FN3	≥5	60	40	100	0.63(6)	–	–	≤50	≤4	≥20
		(40–80)	(30–50)	(90–200)		–	–			
FN4	3	100	40	100	0.60 (2)	24	300	100	10	10
	(2–7)	(70–200)	(8–50)	(30–200)		(10–42)	(60–400)	(20–500)	(2–40)	(3–50)
FN5	5	30	30	30	0.42 (5)	6	20	20	3	30
	(3–10)	(20–40)	(10–40)	(10–40)		(4–8)	(5–30)	(5–70)	(0.8–10)	(10–100)
FN6	≥4	3	6	6	0.5 (7)	67	40	≤10	≤2	≥30
		(2–4)	(5–7)	(5–7)		(45–93)	(30–50)			
FN7	≥4	4	8	8	0.76 (3)	–	–	≤10	≤10	≥30
		(3–6)	(6–11)	(6–11)		–	–			
FN8	7	30	50	50	0.33 (3)	14	70	20	2	50
	(3–30)	(20–50)	(2–60)	(2–60)		(11–18)	(2–80)	(2–70)	(0.2–10)	(10–500)
FN9	8	160	8	270	1.8 (7)	130	3500	50	0.6	40
	(4–20)	(130–210)	(2–9)	(90–320)		(89–190)	(1200–4200)	(7–600)	(0.1–7)	(5–300)
FN10	≥4	40	20	100	0.19 (3)	7	70	≤60	–	≥20
		(20–60)	(10–30)	(60–200)		(0.1–15)	(3–200)			
FN11	≥6	24	30	60	0.84 (7)	3	16	≤20	≤2	≥50
		(18–31)	(20–35)	(40–70)		(1–4)	(8–23)			
FN12	≥2	30	30	70	1.0 (4)	7	50	≤200	≤20	≥4
		(10–40)	(20–70)	(30–140)		(4–10)	(20–100)			
FN14	≥2	50	6	50	1.2 (8)	72	400	≤300	≤20	≥5
		(30–130)	(4–7)	(40–70)		(49–100)	(300–500)			
FN15	≥8	200	230	500	1.6 (4)	19	900	≤50	≤8	≥50
		(100–300)	(160–420)	(300–900)		(15–24)	(700–2000)			
FN16	3	40	10	25	1.1 (5)	6	14	90	20	10
	(2–7)	(20–60)	(5–20)	(11–32)		(4–8)	(6–20)	(10–300)	(2–50)	(4–70)
FN17	≥7	17	20	40	0.3 (6)	12	50	≤10	≤2	≥60
		(10–23)	(10–40)	(30–80)		(5–43)	(30–160)			
FN18	4	8	4	8	1.3 (3)	41	30	20	3	30
	(2–10)	(4–12)	(0.2–5)	(0.4–10)		(19–97)	(2–60)	(3–70)	(0.5–10)	(8–200)
FN19	–	20	20	30	0.25 (4)	5	10	–	–	–
	–	(10–30)	(10–40)	(20–60)		(2–9)	(6–30)			

Table 3. (Continued)

	kT	EM	Flux†	$L_{X(2\text{–}20)}$‡	χ^2_ν (d.o.f)	τ_d§	E_{tot}‖	l♯		B**
	(keV)	(10^{54} cm^{-3})	(10^{-10} erg cm^{-2} s^{-1})	(10^{31} erg s^{-1})		(ks)	(10^{35} erg)	($R_\odot$)	(Binary separation)	(G)
FN20	≥6	2.5	50	6	0.92 (5)	6	3	≤5	–	≥70
		(1.8–3.2)	(30–60)	(4–8)		(4–9)	(2–5)			
FN21	≥4	1.0	40	2	0.54 (4)	4	0.9	≤6	≤0.0005	≥40
		(0.6–1.5)	(30–60)	(1–3)		(2–8)	(0.4–1.7)			
FN22	6	2	70	2.8	1.7 (11)	≤5	≤2	4	–	80
	(3–15)	(1–3)	(30–80)	(1.1–3.3)		–	–	(0.7–20)		(20–400)
FN23	6	20	20	30	0.16 (3)	6	20	20	–	50
	(3–30)	(10–40)	(10–30)	(20–40)		(3–14)	(10–40)	(1–80)		(10–700)

*Since statistics are too limited, FN13 is not fitted. Abundances are fixed to the cosmic value, and the absorbing columns are fixed to zero. Errors and lower limits refer to 90% confidence intervals. The parameters kT, EM, Flux, and L_X of FN23 (TWA-7) are from Uzawa et al. (2011).

†Flux in the 2–20 keV band.

‡Absorption-corrected L_X in the 2–20 keV band. Distances are assumed to be the corresponding values in table 1.

§e-folding time derived with light-curve fitting with a burst model (linear rise and exponential decay).

‖Total released energy derived by multiplying L_X by τ_d.

♯Loop length of flare.

**Magnetic field strength.

indicate that radiative cooling explains all the flares in our data set.

4.4.2 Conductive-cooling model

Secondly, we consider the condition where the conductive cooling is dominant, assuming a semicircular loop of the flare with the cross-section of $\pi(l/10)^2$ for the half-length l, which is often observed in solar flares. In this case, τ_{lc} and the conductive cooling time τ_{con} are given by

$$\tau_{lc} \simeq \tau_{con} = \frac{3n_e kT}{10^{-6} T^{7/2} l^{-2}} = 1.3 \times 10^2 \left(\frac{n_e}{10^{11}\ \mathrm{cm}^{-3}}\right) \times \left(\frac{T}{10^7\ \mathrm{K}}\right)^{-5/2} \left(\frac{l}{10^9\ \mathrm{cm}}\right)^2 \mathrm{s}. \quad (6)$$

On the other hand, a fraction of the thermal energy is observed as radiation. The luminosity L_{X_bol} and EM for the temperature T are written as equations (4) and (3), respectively. With the plasma volume of $(\pi/50)l^3$, EM is also written as

$$EM = \frac{\pi}{50} n_e^2 l^3. \quad (7)$$

Combining equations (3), (6), and (7) gives

$$\tau_{lc} \simeq 1.3 \times 10^5 \left(\frac{50}{\pi}\right)^{2/3} \alpha^{-10/3} n_e^{-1/3} \left(\frac{T}{10^7\ \mathrm{K}}\right)^{19/6}. \quad (8)$$

Once both τ_{lc} and L_{X_bol} were parametrized with the temperature T, we inserted dotted lines in figure 5 as their relation for conductive-cooling dominant model. The values of n_e and α are varied independently within the ranges of $10^{10} \lesssim n_e \lesssim 10^{13}$ cm^{-3} and $0.3 \lesssim \alpha \lesssim 3$, respectively. The figure indicates that the model and the data overlap with each other in the given parameter space.

4.4.3 Propagating-flare model

Thirdly, we examine spatially propagating flares, like two-ribbon flares seen on the Sun. The total energy released during a flare via radiation, E_{rad}, is described as

$$E_{rad} \simeq \tau_{lc} L_{X\_bol}. \quad (9)$$

On the other hand, E_{rad} originates from thermal energy confined in the plasma, and the thermal energy comes from stored magnetic energy, E_{mag}. Then, it can be also written as

$$E_{rad} = f E_{mag} = \frac{f B^2 D^3}{8\pi}, \quad (10)$$

where f is the energy conversion efficiency from magnetic energy to that released as radiation, and D is the scale-length

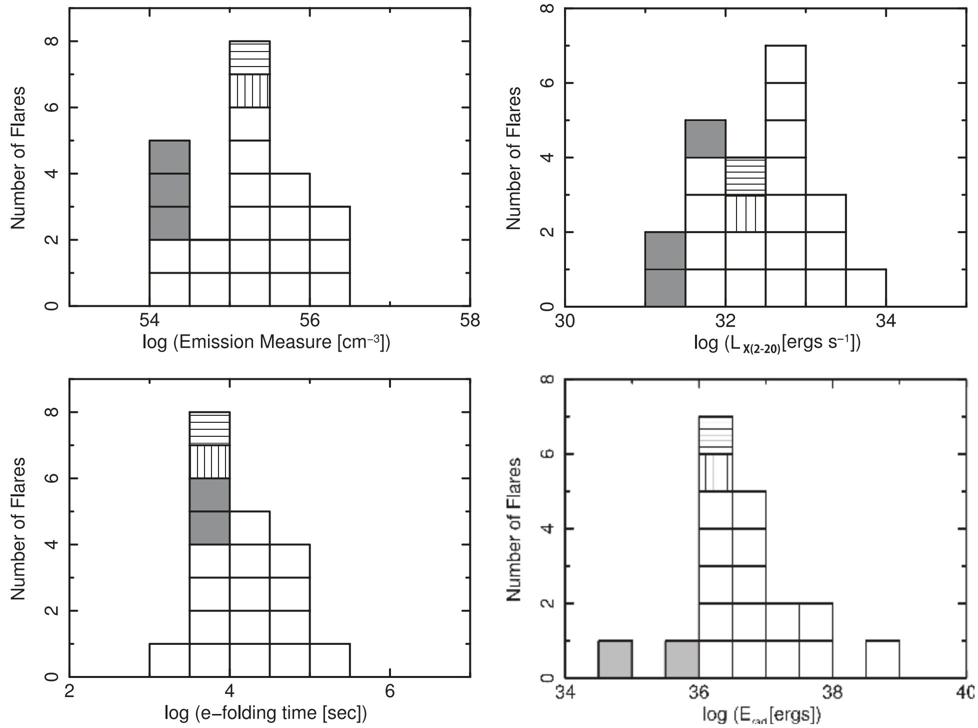

Fig. 3. Distributions of the emission measure (top left), X-ray luminosity in the 2–20 keV band (top right), *e*-folding time (bottom left), and total energy (bottom right). The open squares, filled squares, vertical-striped square, and horizontal-striped square show RS-CVn type stars, dMe stars, Algol, and TWA-7, respectively.

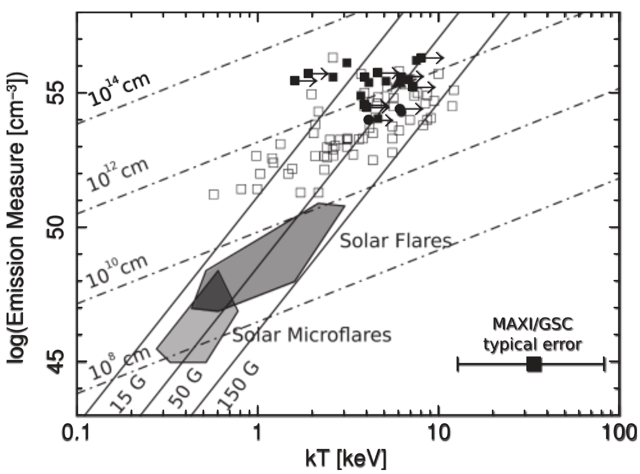

Fig. 4. Log–log plot of emission measure (*EM*) vs. plasma temperature (*kT*) for the MAXI X-ray flares (filled symbols, as in figure 2), along with stellar flares from RS-CVn type, Algol, dMe stars, and YSOs (open squares; the references given in table 4), solar flares (Feldman et al. 1995), and solar microflares (Shimizu 1995). The arrows indicate the lower limits for individual MAXI/GSC sources. The typical error for MAXI/GSC sources in the 90% confidence level is indicated at the right-hand lower corner. The three solid lines are the theoretical *EM*–*kT* relation, based on the equation [$EM \propto B^{-5} T^{17/2}$], for $B = 15$, 50, and 150 gauss and the four dash–dotted lines are that based on the equation [$EM \propto l^{5/3} T^{8/3}$] for the loop-sizes of 10^8, 10^{10}, 10^{12}, and 10^{14} cm (Shibata & Yokoyama 1999).

of the flaring region. When we assume that the magnetic reconnection propagates with the speed v, $\tau_{\rm lc}$ satisfies the following formula

$$\tau_{\rm lc} = D/v. \tag{11}$$

Eliminating $E_{\rm rad}$ and D with the equations (9), (10), and (11), we obtain

$$\tau_{\rm lc} \simeq 1.2 \times 10^4 \left(\frac{f}{0.1}\right)^{1/2} \left(\frac{B}{50\ \rm G}\right)^{-1} \times \left(\frac{v}{3 \times 10^7\ \rm cm\ s^{-1}}\right)^{-3/2} \left(\frac{L_{\rm X\_bol}}{10^{33}\ \rm erg\ s^{-1}}\right)^{1/2} \rm s. \tag{12}$$

If the values of f, B, and v are common among stars,

$$\tau_{\rm lc} \propto L_{\rm X\_bol}^{1/2}. \tag{13}$$

The power of $L_{\rm X\_bol}$ is slightly larger than what we obtained.

4.5 Origin of large flares

4.5.1 Rotation velocity

The positive correlation between quiescent X-ray luminosity and rotation velocity has been reported by Pallavicini (1989) and in subsequent studies. However, no studies have been published about this type of correlation for the flare

Table 4. References for figures 4, 5, 6, and 8.

Reference	Figures	Reference	Figures	Reference	Figures
Alekseev and Kozlova (2001)	6	Jeffries and Bedford (1990)	4, 6, 8	Pettersen (1989)	8
Amado et al. (2000)	8	Kahler et al. (1982)	4, 6	Pizzolato et al. (2003)	6
Anders et al. (1999)	6	Kamata et al. (1997)	4	Poletto, Pallavicini, and Kopp (1988)	4
Benedict et al. (1998)	6	Kjurkchieva, Marchev, and Ogloza (2000)	6	Preibisch, Zinnecker, and Schmitt (1993)	4
Bopp et al. (1989)	8	Kovári et al. (2001)	6	Preibisch, Neuhaeuser, and Alcala (1995)	4
Briggs and Pye (2003)	4	Kuerster and Schmitt (1996)	4, 6, 8	Pribulla et al. (2001)	6, 8
Covino et al. (2001)	4, 6, 8	Landini et al. (1986)	4, 8	Pye and McHardy (1983)	5, 6
Demory et al. (2009)	6, 8	Lim, Vaughan, and Nelson (1987)	8	Qian et al. (2002)	8
Dempsey et al. (1993)	6	Linsky (1991)	5	Ramseyer, Hatzes, and Jablonski (1995)	6
Donati (1999)	8	Linsky et al. (2001)	8	Randich, Gratton, and Pallavicini (1993)	6
Donati et al. (1997)	6	Maggio et al. (2000)	4, 5, 6, 8	Reiners and Basri (2007)	6
Doyle et al. (1988)	4	Mewe et al. (1997)	4	Reiners, Basri, and Browning (2009)	6
Duemmler and Aarum (2001)	6, 8	Miranda, Vaccaro, and Oswalt (2007)	8	Robinson et al. (2003)	6
Eaton and Henry (2007)	6, 8	Mitra-Kraev (2007)	6	Sanz-Forcada, Brickhouse, and Dupree (2003)	6, 8
Endl, Strassmeier, and Kurster (1997)	4, 6, 8	Mitra-Kraev (2007)	6	Singh, Drake, and White (1995)	6
ESA (1997)	5, 6	Miura et al. (2008)	5	Stawikowski and Glebocki (1994)	6
Favata and Schmitt (1999)	4	Montes et al. (1995)	6	Stern, Underwood, and Antiochos (1983)	4
Favata et al. (2000a)	5	Montmerle et al. (1983)	4	Stern et al. (1992)	5
Favata, Micela, and Reale (2000b)	4, 6, 8	Morales et al. (2009)	8	Strassmeier et al. (1993)	6
Favata, Micela, and Reale (2001)	4, 6, 8	Morin et al. (2008)	6, 8	Strassmeier, Paunzen, and North (1994)	6, 8
Fekel et al. (1999)	6, 8	Murdoch et al. (1995)	8	Strassmeier and Rice (1998)	6, 8
Franciosini, Pallavicini, and Tagliaferri (2001)	4, 5	O'Brien, Bond, and Sion (2001)	6, 8	Strassmeier and Rice (2003)	6
Frasca, Catalano, and Mantovani (1997)	6	O'Neal et al. (2001)	6, 8	Torres and Ribas (2002)	6, 8
Güdel et al. (1999)	4	Osten and Saar (1998)	6	Tsuboi et al. (1998)	4, 5, 8
Güdel et al. (2004)	4, 6, 8	Osten et al. (2007)	5	Tsuboi et al. (2000)	4
Gagne, Caillault, and Stauffer (1995)	4	Osten et al. (2010)	4, 5, 6, 8	Tsuru et al. (1989)	4
Glebocki and Stawikowski (1995)	6	Ottmann and Schmitt (1994)	4	van den Oord, Mewe, and Brinkman (1988)	4, 6, 8
Gunn, Mitrou, and Doyle (1998)	8	Ozawa et al. (1999)	4	van den Oord and Mewe (1989)	6, 8
Hamaguchi et al. (2000)	4	Pallavicini, Tagliaferri, and Stella (1990a)	4, 5, 6, 8	Welty (1995)	6, 8
Hatzes (1995)	6	Pallavicini et al. (1990b)	4	White, Lim, and Kundu (1994)	8
Huensch and Reimers (1995)	4	Pan and Jordan (1995)	4, 6, 8	Wright et al. (2011)	6, 8
Hussain et al. (2005)	6	Pan et al. (1997)	4, 5, 8	Yang, Johns-Krull, and Valenti (2008)	6, 8
Imanishi et al. (2001)	4	Pandey and Singh (2008)	4, 5, 6, 8	Zboril et al. (2005)	6, 8
Imanishi et al. (2003)	5	Pettersen (1980)	6		

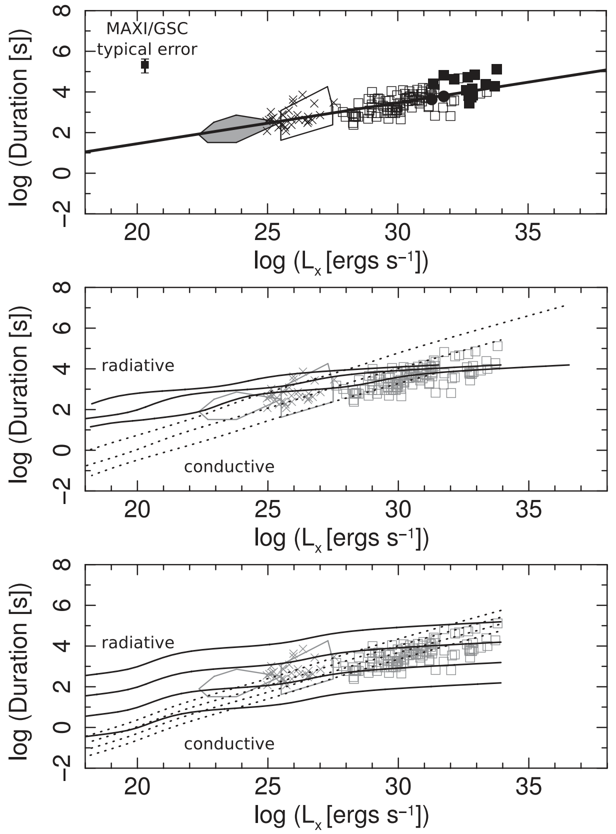

Fig. 5. Top panel: Log–log plot of the duration of flare vs. the X-ray luminosity in the 0.1–100 keV band. Our best-fitting model is inserted with a broad solid line. The filled and open symbols are the same as those in figure 2 and 4, respectively. We superpose three sets of data of solar flares: X marks, a large open pentagon, and a large gray region, taken from Pallavicini, Serio, and Vaiana (1977), Veronig et al. (2002), and Shimizu (1995), respectively. The typical error for MAXI/GSC sources is also inserted. Middle panel: The theoretical relations of the radiative-cooling model (solid line) and conductive-cooling model (dotted line) are overlaid for the non-dimensional parameter α of 0.3, 1, and 3 from the top to bottom lines, respectively, for both the models, where n_e is fixed to 10^{11} cm^{-3}. Bottom panel: Same as the middle panel, but with α fixed to 1 and n_e varied instead for $n_e = 10^{10}$, 10^{11}, 10^{12}, and 10^{13} cm^{-3}, corresponding to the four lines from top to bottom, respectively, for each model.

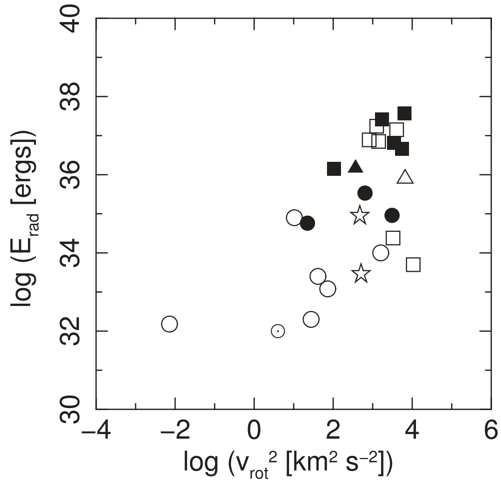

Fig. 6. Log–log plot of total energy released radiatively in a flare vs. the square of rotation velocity. The filled symbols are the same as those in figure 2. The open squares, open circles, open triangles, open stars, and an open circle with a dot show the values obtained in previous studies for RS-CVn type stars, dMe stars, YSOs, dKe stars, and the Sun, respectively. If flares have been detected from a source with MAXI or the other missions more than once, only the largest E_{rad} is plotted. For the rotation velocity, if the flare source is a multiple-star system, we used the value of the component which has the largest stellar radius.

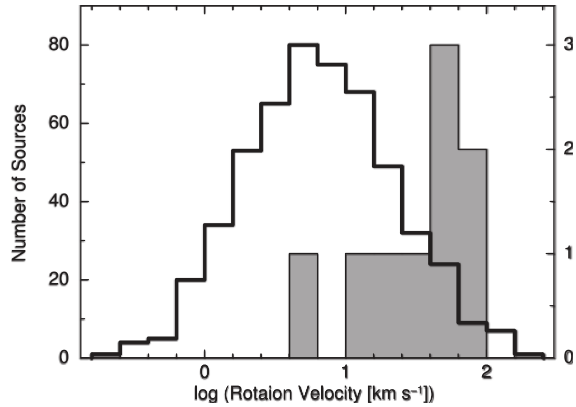

Fig. 7. Histogram of rotation velocities. The gray bars indicate the MAXI/GSC-detected sources within 100 pc with the scale (0–3) displayed on the right-hand *y*-axis. The white bars indicate active binaries and X-ray-detected stellar sources both within 100 pc (from Eker et al. 2008 and Wright et al. 2011), with the scale displayed on the left-hand *y*-axis, from which the MAXI/GSC-detected sources are excluded.

luminosity. Compiling our data sample and those in literature, we search for potential correlations of this kind.

We plot the total energy released during a flare (i.e., E_{rad}) vs. the square of rotation velocity (v_{rot}^2) in figure 6, where E_{rad} is derived by multiplying L_X in the 2–20 keV band by the *e*-folding time of the flare-decaying phase.[8] From figure 6, we find that the MAXI sample is concentrated at the region of the high rotation velocity and the large total energy. This is the first indication with an unbiased survey that stellar sources with higher rotation velocities can have a very high E_{rad}.

In order to validate this tendency further, we made two histograms of the number of sources as a function of the star-rotation velocity for flare sources. One is for our MAXI/GSC sample, and the other is for cataloged nearby stars from the literature (active binaries, Eker et al. 2008; X-ray-detected stellar sources, Wright et al. 2011). Both the samples are within 100 pc distance, and from the latter sample, MAXI/GSC sources are excluded. Figure 7 shows the two histograms. The MAXI/GSC sources have

[8] If flares have been detected from a source multiple times with MAXI and/or other missions, only the largest total energy is used. If the flare source is a multiple-star system, we use the rotation velocity of the star with the largest stellar radius in the system. In our sample, the source with the largest radius has a higher velocity than the other stars in the same system for all the multiple-star systems except EQ Peg.

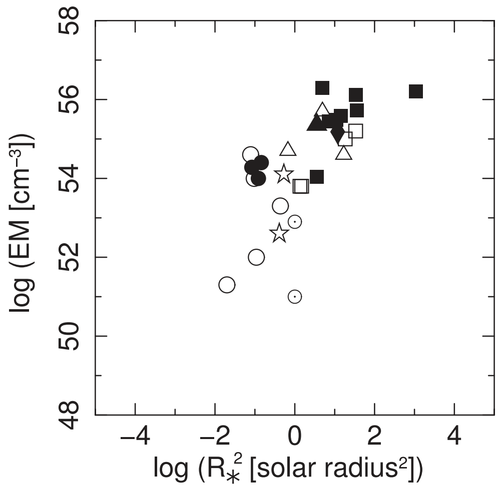

Fig. 8. Log–log plot of emission measure vs. square of radius. The symbols are the same as in figure 6. The upper open circle with a dot indicates π^1 UMa, while the lower open one with a dot indicates the Sun.

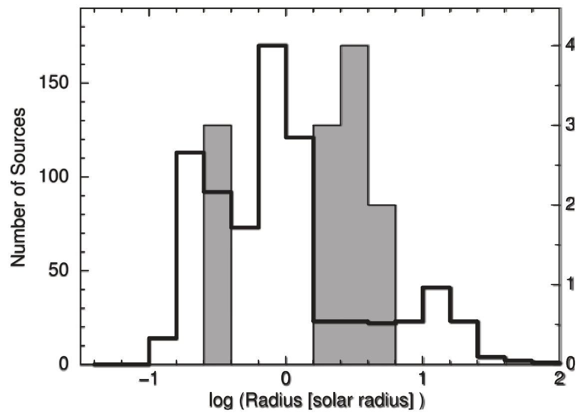

Fig. 9. Histogram of stellar radii. The gray bars indicate the MAXI/GSC sources within 100 pc with the scale (0–4) displayed on the right-hand *y*-axis. The white bars indicate active binaries and X-ray-detected stellar sources both within 100 pc (from Eker et al. 2008 and Wright et al. 2011), with the scale displayed on the left-hand *y*-axis, from which the MAXI/GSC-detected sources are excluded.

the median logarithmic rotation velocity of 1.52 in units of log (km s^{-1}) with the standard deviation of 0.37 dex. On the other hand, the undetected sources with MAXI/GSC have the median logarithmic value of 0.80 in the same units with the standard deviation of 0.52 dex. Therefore, the rotation velocities of the MAXI sources, which have shown huge flares as reported in this paper, are significantly higher than those of the other active stars that are comparatively quiet. This supports that the sources with faster velocities generate larger flares.

4.5.2 Stellar radius

We investigate whether the MAXI sources and/or the size of the flare-emitting region have any common characteristics or correlations in their stellar radii.

Figure 8 plots *EM* vs. the square of the stellar radius (R_*^2) for the stars detected with MAXI/GSC and those detected with other missions (see table 4 for the complete set of references).[9] Though the sample is limited, a hint of the positive correlation between *EM* and R_*^2 is seen at least in the MAXI/GSC sources.[10]

We also made a number-distribution histogram as a function of the radius in figure 9, similar to figure 7. In figure 9, we find MAXI/GSC sources are concentrated at the radii of about 3 and 0.3 $R_\odot$, which correspond to those of RS CVn-type and dMe stars, respectively. On the other hand, the undetected sources with MAXI/GSC are widely distributed in figure 9, which implies that the magnitude of flares is not as sensitive to the stellar radius as to the rotation velocity.

[9] The largest *EM* is used for each source if flares have been detected multiple times, and the radius of the larger star is used if the source is a multiple-star system.

[10] For the flares detected with Ariel-V/SSI, Rao and Vahia (1987) have made the similar plot, which shows a similar correlation to ours, although their plot was the bolometric luminosity vs. the X-ray peak luminosity.

5 Summary

(1) During the two-year MAXI/GSC survey, we detected 23 energetic flares from 13 active stars (eight RS-CVn stars, three dMe stars, one YSO, and one Algol type star). The physical parameters of the flares are very large for stellar flares in all of the following characteristics: the X-ray luminosity L_X (10^{31-34} erg s^{-1} in the 2–20 keV band), the emission measure *EM* (10^{54-57} cm^{-3}), the *e*-folding time (10^{3-6} s), and the total energy released during the flare (10^{34-39} erg).

(2) The flares from GT Mus, V841 Cen, SZ Psc, and TWA-7 were detected for the first time in the X-ray band. From II Peg, we detected one of the largest flares among stellar flares with L_X of $5^{+4}_{-2} \times 10^{33}$ erg s^{-1} in the 2–20 keV band. Whereas most of the sources detected with MAXI/GSC are multiple-star systems, two of them (YZ CMi and TWA-7) are single and are known to have no accretion disk. These results reinforce the scenario that neither binarity, nor accretion, nor star-disk interaction is essential to generate large flares, as already discussed in Uzawa et al. (2011).

(3) The survey showed the number of the sources that show extremely large flares is very limited; that is, only 10 out of the 256 active binaries within the 100 pc distance have been detected, while four of the 10 sources showed flares multiple times. We detected no X-ray flares from solar-type stars, despite the fact that 15 G-type main-sequence stars lie within the 10 pc distance. This implies that the frequency of the superflares from solar-type stars, which have L_X of more than 1×10^{30} erg s^{-1}, is very small.

(4) On the EM–kT plot, our sample is located at the high ends in the universal correlation, which ranges over orders of magnitude (Feldman et al. 1995; Shibata & Yokoyama 1999). According to the theory of Shibata and Yokoyama (1999), our sample has a similar intensity of magnetic field to those detected on the Sun (∼15–150 G), but has flare-loop sizes that are orders of magnitude larger than those on the Sun ($< 0.1\ R_\odot$). The largest two loop sizes from UX Ari and II Peg are huge, and are much larger than their binary separations.

(5) We plotted the duration vs. $L_{\mathrm{X\_bol}}$, using the data of solar and stellar flares in literature and the data of the flares on MAXI/GSC sources. The plot indicates that there is a universal positive correlation between the $L_{\mathrm{X\_bol}}$ of a flare and its duration, such that a longer duration means a higher $L_{\mathrm{X\_bol}}$. The correlation holds for the wide range of parameter values; 12 and 5 orders of magnitude in $L_{\mathrm{X\_bol}}$ and duration, respectively. Our sample is located at the highest ends on the correlation. From the data, we found that the duration is proportional to $L_{\mathrm{X\_bol}}^{0.2}$.

(6) Our sample has especially fast rotation velocities, of the order of 10 km s^{-1}. This indicates that the rotation velocity is an essential parameter in generating big flares.

Acknowledgements

We thank M. Sakano, Y. Maeda, F. Reale, and S. Takasao for useful discussion. This research has made use of the MAXI data,[11] provided by the RIKEN, JAXA, and MAXI teams. This research was partially supported by the Ministry of Education, Culture, Sports, Science and Technology (MEXT), Grant-in-Aid Nos.19047001, 20041008, 20244015, 20540230, 20540237, 21340043, 21740140, 22740120, 23540269, 16K17667, and Global-COE from MEXT "The Next Generation of Physics, Spun from Universality and Emergence" and "Nanoscience and Quantum Physics". Y.T. acknowledges financial support by a Chuo University Grant for Special Research.

Appendix. The process to derive $L_{\mathrm{X\_bol}}$ for each data set

In subsection 4.4, we derived the intrinsic X-ray luminosity $L_{\mathrm{X\_bol}}$ in the 0.1–100 keV band from the available observed X-ray data in narrower energy bands (Pallavicini et al. 1977; Shimizu 1995; Veronig et al. 2002). The process to derive it is as follows.

(1) In principle, we derive $L_{\mathrm{X\_bol}}$ from the parameters kT and EM, using equation (4). As for the X-ray data of Shimizu (1995) and Veronig et al. (2002), it is necessary to estimate the values of kT and EM from the X-ray luminosities in the GOES band (3.1–24.8 keV) (hereafter $L_{\mathrm{X\_GOES}}$). To estimate them, first, we derive the ratios [denoted as $P(T)$] of the X-ray luminosity in the GOES band to that in the 0.1–100 keV band (i.e., $L_{\mathrm{X\_bol}}$) as a function of kT, using the *apec* model in *XSPEC*. Next, assuming the empirical relation of EM vs. kT for flares [equation (3)], we obtain EM as a function of kT, with the parameter α fixed to 1 [hereafter $EM(T)$]. Combining these parameters with equation (4), the GOES band luminosity is written as

$$L_{\mathrm{X\_GOES}} = L_{\mathrm{X\_bol}}\, P(T) = F(T)\, EM(T)\, P(T). \qquad \text{(A1)}$$

We can derive T for each $L_{\mathrm{X\_GOES}}$, and then obtain $L_{\mathrm{X\_bol}}$ by this formula.

(2) As for the X-ray data of Pallavicini, Tagliaferri, and Stella (1990a), we simply accept the X-ray luminosities in the 0.05–2 keV band in their paper as $L_{\mathrm{X\_bol}}$, because the luminosities in the band are estimated to be about 95% of $L_{\mathrm{X\_bol}}$. Note that we have used the *apec* model in *XSPEC*, varying the temperatures in the range of $\log T = 6.5$–7.3 (K), to get the ratio of 95%, where the range for the temperatures is assumed by Pallavicini, Tagliaferri, and Stella (1990a).

[11] ⟨http://maxi.riken.jp/top/index.php⟩.

References

Alekseev, I. Y., & Kozlova, O. V. 2001, Astrophys., 44, 429
Amado, P. J., Doyle, J. G., Byrne, P. B., Cutispoto, G., Kilkenny, D., Mathioudakis, M., & Neff, J. E. 2000, A&A, 359, 159
Anders, G. J., Coates, D. W., Thompson, K., & Innis, J. L. 1999, MNRAS, 310, 377
Argiroffi, C., et al. 2011, A&A, 530, A1
Benedict, G. F., et al. 1998, AJ, 116, 429
Berdyugina, S. V., Jankov, S., Ilyin, I., Tuominen, I., & Fekel, F. C. 1998, A&A, 334, 863
Bopp, B. W., Saar, S. H., Ambruster, C., Feldman, P., Dempsey, R., Allen, M., & Barden, S. C. 1989, ApJ, 339, 1059
Briggs, K. R., & Pye, J. P. 2003, MNRAS, 345, 714
Cargill, P. J., & Klimchuck, J. A. 2004, ApJ, 605, 911
Carlos, R. C., & Popper, D. M. 1971, PASP, 83, 504
Castro-Tirado, A. J., Brandt, S., Lund, N., & Sunyaev, R. 1999, A&A, 347, 927
Chambliss, C. R. 1976, PASP, 88, 762
Christe, S., Hannah, I. G., Krucker, S., McTiernan, J., & Lin, R. P. 2008, ApJ, 677, 1385
Collier, A. C. 1982, PhD thesis, University of Canterbury
Covino, S., Panzera, M. R., Tagliaferri, G., & Pallavicini, R. 2001, A&A, 371, 973
Demory, B.-O., et al. 2009, A&A, 505, 205
Dempsey, R. C., Bopp, B. W., Henry, G. W., & Hall, D. S. 1993, ApJS, 86, 293
Donati, J.-F. 1999, MNRAS, 302, 457
Donati, J.-F., Semel, M., Carter, B. D., Rees, D. E., & Collier Cameron, A. 1997, MNRAS, 291, 658
Doyle, J. G., Butler, C. J., Callanan, P. J., Tagliaferri, G., de La Reza, R., White, N. E., Torres, C. A., & Quast, G. 1988, A&A, 191, 79

Duemmler, R., & Aarum, V. 2001, A&A, 370, 974
Eaton, J. A., & Henry, G. W. 2007, PASP, 119, 259
Eker, Z., et al. 2008, MNRAS, 389, 1722
Endl, M., Strassmeier, K. G., & Kurster, M. 1997, A&A, 328, 565
ESA 1997, ESA-SP 1200, The Hipparcos and Tycho Catalogues (Noordwijk: ESA)
Favata, F., & Micela, G. 2003, Space Sci. Rev., 108, 577
Favata, F., Micela, G., & Reale, F. 2000b, A&A, 354, 1021
Favata, F., Micela, G., & Reale, F. 2001, A&A, 375, 485
Favata, F., Reale, F., Micela, G., Sciortino, S., Maggio, A., & Matsumoto, H. 2000a, A&A, 353, 987
Favata, F., & Schmitt, J. H. M. M. 1999, A&A, 350, 900
Fekel, F. C., Strassmeier, K. G., Weber, M., & Washuettl, A. 1999, A&AS, 137, 369
Fekel, F. C., Jr. 1983, ApJ, 268, 274
Feldman, U., Laming, J. M., & Doschek, G. A. 1995, ApJ, 451, L79
Franciosini, E., Pallavicini, R., & Tagliaferri, G. 2001, A&A, 375, 196
Frasca, A., Catalano, S., & Mantovani, D. 1997, A&A, 320, 101
Gagne, M., Caillault, J.-P., & Stauffer, J. R. 1995, ApJ, 450, 217
Getman, K. V., Broos, P. S., Salter, D. M., Garmire, G. P., & Hogerheijde, M. R. 2011, ApJ, 730, 6
Glebocki, R., & Stawikowski, A. 1995, Acta Astron., 45, 725
Güdel, M. 2004, A&A Rev., 12, 71
Güdel, M., Audard, M., Reale, F., Skinner, S. L., & Linsky, J. L. 2004, A&A, 416, 713
Güdel, M., Audard, M., Skinner, S. L., & Horvath, M. I. 2002, ApJ, 580, L73
Güdel, M., Linsky, J. L., Brown, A., & Nagase, F. 1999, ApJ, 511, 405
Gunn, A. G., Mitrou, C. K., & Doyle, J. G. 1998, MNRAS, 296, 150
Haisch, B., Strong, K. T., & Rodono, M. 1991, ARA&A, 29, 275
Hamaguchi, K., Terada, H., Bamba, A., & Koyama, K. 2000, ApJ, 532, 1111
Hatzes, A. P. 1995, AJ, 109, 350
Hayashi, M. R., Shibata, K., & Matsumoto, R. 1996, ApJ, 468, L37
Hopmann J. 1958, Mitt. Sternw. Wien, 9, 127
Huensch, M., & Reimers, D. 1995, A&A, 296, 509
Hussain, G. A. J., Brickhouse, N. S., Dupree, A. K., Jardine, M., van Ballegooijen, A., Collier Cameron, A., Donati, J.-F., & Favata, F. 2005, ESA-SP 560, Proceedings of the 13th Cambridge Workshop on Cool Stars, Stellar Systems and the Sun, ed. F. Favata & G. A. J. Hussain (Noordwijk, ESA), 665
Imanishi, K., Koyama, K., & Tsuboi, Y. 2001, in ASP Conf. Ser., 251, New Century of X-ray Astronomy, ed. H. Inoue & H. Kunieda (San Francisco: ASP), 246
Imanishi, K., Nakajima, H., Tsujimoto, M., Koyama, K., & Tsuboi, Y. 2003, PASJ, 55, 653
Jakate, S., Bakos, G. A., Fernie, J. D., & Heard, J. F. 1976, AJ, 81, 250
Jeffries, R. D., & Bedford, D. K. 1990, MNRAS, 246, 337
Kaastra, J. S. 1992, An X-Ray Spectral Code for Optically Thin Plasmas (Internal SRON-Leiden Report, updated version 2.0)
Kahler, S., et al. 1982, ApJ, 252, 239
Kamata, Y., Koyama, K., Tsuboi, Y., & Yamauchi, S. 1997, PASJ, 49, 461
Kastner, J. H., Huenemoerder, D. P., Schulz, N. S., Canizares, C. R., & Weintraub, D. A. 2002, ApJ, 567, 434
Kjurkchieva, D., Marchev, D., & Ogloza, W. 2000, A&A, 354, 909
Kovári, Z., Strassmeier, K. G., Bartus, J., Washuettl, A., Weber, M., & Rice, J. B. 2001, A&A, 373, 199
Krimm, H. A., et al. 2013, ApJS, 209, 14
Kuerster, M., & Schmitt, J. H. M. M. 1996, A&A, 311, 211
Landini, M., Monsignori Fossi, B. C., Pallavicini, R., & Piro, L. 1986, A&A, 157, 217
Lanza, A. F., Piluso, N., Rodonò, M., Messina, S., & Cutispoto, G. 2006, A&A, 455, 595
Liedahl, D. A., Osterheld, A. L., & Goldstein, W. H. 1995, ApJ, 438, L115
Lim, J., Vaughan, A. E., & Nelson, G. J. 1987, Proc. Astron. Soc. Aust., 7, 197
Linsky, J. L. 1991, Mem. Soc. Astron. Ital., 62, 307
Linsky, J. L., Skinner, S., Osten, R., & Gagné, M. 2001, in ASP Conf. Ser., 248, Magnetic Fields Across the Hertzsprung-Russell Diagram, ed. G. Mathys (San Francisco: ASP), 255
López-Santiago, J., Montes, D., Crespo-Chacón, I., & Fernández-Figueroa, M. J. 2006, ApJ, 643, 1160
Maggio, A., Pallavicini, R., Reale, F., & Tagliaferri, G. 2000, A&A, 356, 627
Mamajek, E. E. 2005, ApJ, 634, 1385
Marino, G., Rodonó, M., Leto, G., & Cutispoto, G. 1999, A&A, 352, 189
Matsuoka, M., et al. 2009, PASJ, 61, 999
Mewe, R., Gronenschild, E. H. B. M., & van den Oord, G. H. J. 1985, A&AS, 62, 197
Mewe, R., Kaastra, J. S., van den Oord, G. H. J., Vink, J., & Tawara, Y. 1997, A&A, 320, 147
Mewe, R., Lemen, J. R., & van den Oord, G. H. J. 1986, A&AS, 65, 511
Mihara, T., et al. 2011, PASJ, 63, S623
Miranda, V., Vaccaro, T., & Oswalt, T. D. 2007, J. Southeastern Assoc. Res. Astron., 1, 17
Mitra-Kraev, U. 2007, Observatory, 127, 360
Mitra-Kraev, U., et al. 2005, A&A, 431, 679
Miura, J., Tsujimoto, M., Tsuboi, Y., Maeda, Y., Sugawara, Y., Koyama, K., & Yamauchi, S. 2008, PASJ, 60, S49
Montes, D., Fernandez-Figueroa, M. J., de Castro, E., & Cornide, M. 1995, A&A, 294, 165
Montmerle, T., Grosso, N., Tsuboi, Y., & Koyama, K. 2000, ApJ, 532, 1097
Montmerle, T., Koch-Miramond, L., Falgarone, E., & Grindlay, J. E. 1983, ApJ, 269, 182
Morales, J. C., Torres, G., Marschall, L. A., & Brehm, W. 2009, ApJ, 707, 671
Morii, M., et al. 2010, in AIP Conf. Proc., 1279, Deciphering the Ancient Universe with Gamma-Ray Bursts, ed. N. Kawai & S. Nagataki (New York: AIP), 391
Morin, J., et al. 2008, MNRAS, 390, 567
Murdoch, K. A., Hearnshaw, J. B., Kilmartin, P. M., & Gilmore, A. C. 1995, MNRAS, 276, 836
Negoro, H., et al. 2016 PASJ, 68, S1
Negoro, H., et al. 2010, in AIP Conf. Proc., 1248, X-ray Astronomy 2009; Present Status, Multi-Wavelength Approach and Future Perspectives, ed. A. Comastri et al. (New York: AIP), 589

O'Brien, M. S., Bond, H. E., & Sion, E. M. 2001, in ASP Conf. Ser., 226, 12th European Workshop on White Dwarfs, ed. J. L. Provencal et al. (San Francisco: ASP), 240
O'Neal, D., Neff, J. E., Saar, S. H., & Mines, J. K. 2001, AJ, 122, 1954
Osten, R. A., et al. 2010, ApJ, 721, 785
Osten, R. A., Drake, S., Tueller, J., Cummings, J., Perri, M., Moretti, A., & Covino, S. 2007, ApJ, 654, 1052
Osten, R. A., & Saar, S. H. 1998, MNRAS, 295, 257
Ottmann, R., & Schmitt, J. H. M. M. 1994, A&A, 283, 871
Ozawa, H., Nagase, F., Ueda, Y., Dotani, T., & Ishida, M. 1999, ApJ, 523, L81
Özeren, F. F., Doyle, J. G., & Jevremovic, D. 1999, A&A, 350, 635
Pallavicini, R. 1989, A&A Rev., 1, 177
Pallavicini, R., Serio, S., & Vaiana, G. S. 1977, ApJ, 216, 108
Pallavicini, R., Tagliaferri, G., Pollock, A. M. T., Schmitt, J. H. M. M., & Rosso, C. 1990b, A&A, 227, 483
Pallavicini, R., Tagliaferri, G., & Stella, L. 1990a, A&A, 228, 403
Pan, H. C., & Jordan, C. 1995, MNRAS, 272, 11
Pan, H. C., Jordan, C., Makishima, K., Stern, R. A., Hayashida, K., & Inda-Koide, M. 1997, MNRAS, 285, 735
Pandey, J. C., & Singh, K. P. 2008, MNRAS, 387, 1627
Pettersen, B. R. 1980, AJ, 85, 871
Pettersen, B. R. 1989, A&A, 209, 279
Pettersen, B. R., Coleman, L. A., & Evans, D. S. 1984, ApJ, 282, 214
Pizzolato, N., Maggio, A., Micela, G., Sciortino, S., & Ventura, P. 2003, A&A, 397, 147
Poletto, G., Pallavicini, R., & Kopp, R. A. 1988, A&A, 201, 93
Preibisch, T., Neuhaeuser, R., & Alcala, J. M. 1995, A&A, 304, L13
Preibisch, T., Zinnecker, H., & Schmitt, J. H. M. M. 1993, A&A, 279, L33
Pribulla, T., Chochol, D., Heckert, P. A., Errico, L., Vittone, A. A., Parimucha, Š., & Teodorani, M. 2001, A&A, 371, 997
Pye, J. P., & McHardy, I. M. 1983, MNRAS, 205, 875
Qian, S., Liu, D., Tan, W., & Soonthornthum, B. 2002, AJ, 124, 1060
Ramseyer, T. F., Hatzes, A. P., & Jablonski, F. 1995, AJ, 110, 1364
Randich, S., Gratton, R., & Pallavicini, R. 1993, A&A, 273, 194
Rao, A. R., & Vahia, M. N. 1987, A&A, 188, 109
Reale, F. 2007, A&A, 471, 271
Reale, F., & Micela, G. 1998, A&A, 334, 1028
Reiners, A., & Basri, G. 2007, ApJ, 656, 1121
Reiners, A., Basri, G., & Browning, M. 2009, ApJ, 692, 538
Richards, M. T., Waltman, E. B., Ghigo, F. D., & Richards, D. S. P. 2003, ApJS, 147, 337
Riedel, A. R., et al. 2014, AJ, 147, 85
Robinson, R. D., Ake, T. B., Dupree, A. K., & Linsky, J. L. 2003, Proc. 12th Cambridge Workshop on Cool Stars, Stellar Systems, and the Sun: The Future of Cool-Star Astrophysics, ed. A. Brown et al. (Boulder: University of Colorado), 964
Sanford, R. F. 1951, ApJ 113, 299
Sanz-Forcada, J., Brickhouse, N. S., & Dupree, A. K. 2003, ApJS, 145, 147
Sarna, M. J. 1993, MNRAS, 262, 534
Schaefer, B. E., King, J. R., & Deliyannis, C. P. 2000, ApJ, 529, 1026
Shibata, K., & Yokoyama, T. 1999, ApJ, 526, L49
Shibata, K., & Yokoyama, T. 2002, ApJ, 577, 422
Shimizu, T. 1995, PASJ, 47, 251
Shu, F. H., Shang, H., Glassgold, A. E., & Lee, T. 1997, Science, 277, 1475
Singh, K. P., Drake, S. A., & White, N. E. 1995, ApJ, 445, 840
Smith, R. K., Brickhouse, N. S., Liedahl, D. A., & Raymond, J. C. 2001, ApJ, 556, L91
Söderhjelm, S. 1999, A&A, 341, 121
Stawikowski, A., & Glebocki, R. 1994, Acta Astron., 44, 393
Stern, R. A., Uchida, Y., Tsuneta, S., & Nagase, F. 1992, ApJ, 400, 321
Stern, R. A., Underwood, J. H., & Antiochos, S. K. 1983, ApJ, 264, L55
Strassmeier, K. G., Hall, D. S., Fekel, F. C., & Scheck, M. 1993, A&AS, 100, 173
Strassmeier, K. G., Paunzen, E., & North, P. 1994, IBVS, 4066, 1
Strassmeier, K. G., & Rice, J. B. 1998, A&A, 339, 497
Strassmeier, K. G., & Rice, J. B. 2003, A&A, 399, 315
Sugizaki, M., et al. 2011, PASJ, 63, S635
Tomida, H., et al. 2011, PASJ, 63, 397
Torres, C. A. O., Quast, G. R., da Silva, L., de la Reza, R., Melo, C. H. F., & Sterzik, M. 2006, VizieR Online Data Catalog, J/A+A/460/695
Torres, G., & Ribas, I. 2002, ApJ, 567, 1140
Tsuboi, Y., Imanishi, K., Koyama, K., Grosso, N., & Montmerle, T. 2000, ApJ, 532, 1089
Tsuboi, Y., Koyama, K., Murakami, H., Hayashi, M., Skinner, S., & Ueno, S. 1998, ApJ, 503, 894
Tsunemi, H., Tomida, H., Katayama, H., Kimura, M., Daikyuji, A., Miyaguchi, K., Maeda, K., & MAXI Team, 2010, PASJ, 62, 1371
Tsuru, T., et al. 1989, PASJ, 41, 679
Uzawa, A., et al. 2011, PASJ, 63, S713
van den Oord, G. H. J., & Mewe, R. 1989, A&A, 213, 245
van den Oord, G. H. J., Mewe, R., & Brinkman, A. C. 1988, A&A, 205, 181
Veronig, A., Temmer, M., Hanslmeier, A., Otruba, W., & Messerotti, M. 2002, A&A, 382, 1070
Voges, W., et al. 1999, A&A, 349, 389
Vogt, S. S. 1981, ApJ, 247, 975
Welty, A. D. 1995, AJ, 110, 776
White, S. M., Lim, J., & Kundu, M. R. 1994, ApJ, 422, 293
Wilson, O. C. 1978, ApJ, 226, 379
Wright, N. J., Drake, J. J., Mamajek, E. E., & Henry, G. W. 2011, ApJ, 743, 48
Yang, H., Johns-Krull, C. M., & Valenti, J. A. 2008, AJ, 136, 2286
Yokoyama, T., & Shibata, K. 1998, ApJ, 494, L113
Zboril, M., Oliveira, J. M., Messina, S., Djurašević, G., & Amado, P. J. 2005, Contrib. Astron. Obs. Skalnaté Pleso, 35, 23